



A non-spherical model for bubble formation with liquid cross-flow

R. B. H. Tan*, W. B. Chen, K. H. Tan

Department of Chemical and Environmental Engineering, National University of Singapore, 10 Kent Ridge Crescent, Singapore 119260, Singapore

Received 21 March 2000; received in revised form 20 June 2000; accepted 4 July 2000

Abstract

A non-spherical model for bubble formation at an orifice with liquid cross-flow has been developed. The interface element approach is applied to describe the dynamics of bubble formation. The effect of liquid cross-flow on the bubble formation process is modelled by a combination of tilting of the bubble axis and liquid pressure analysis of each element on the bubble interface. Model predictions compare well with the experimental results available in the literature for different conditions of gas flow rate, orifice diameter and liquid cross-flow velocity. Simulated bubble shapes are highly non-spherical, especially at high liquid velocities, and bear a striking resemblance with the experimental high-speed video sequences. © 2000 Elsevier Science Ltd. All rights reserved.

Keywords: Bubble formation; Orifice; Non-spherical model; Cross-flow; Tilted axis; Liquid pressure

1. Introduction

The dispersion of gases through submerged orifices, slots or holes is an efficient and commonly used method of creating large interfacial area per unit volume in process equipment such as distillation columns, absorption towers, flotation cells, aerated stirred tanks, biological wastewater treatment systems and metallurgical smelters. In many industrial gas–liquid operations, the continuous phase is caused to flow normally across the emerging gas at the orifices either by bulk liquid motion tangential to the orifice or by motion of the orifices as in gas-sparged impellers or rotary spargers. Bubble formation under such conditions of liquid cross-flow is known to produce smaller bubbles when compared with formation under stagnant or quiescent liquid conditions. Another advantage of cross-flowing liquids is that the detached bubbles tend to be swept away from the region of the orifice, thereby reducing the likelihood of coalescence.

Maier's (1927) pioneering work demonstrated that the shear force experienced by a growing bubble in a flowing liquid, which causes its premature detachment, is a maximum when the liquid flows at right angles to the nozzle axis. Stich and Barr (1979) studied the effect of liquid

cross-flow on bubble formation at submerged orifices experimentally, and proposed an empirical correlation for final bubble radius in terms of gas flow rate and liquid cross-flow velocity. Sullivan, Hardy and Holland (1964) developed a semi-empirical model based on expansion, vertical displacement and horizontal displacement of a spherical bubble, the volume of which was correlated to experimental values of Reynolds and Froude numbers. Rigby, Evans and Jameson (1995) studied the mechanisms for gas dispersion from an orifice situated in the region of non-separated flow on the surface of a cylinder immersed in liquid cross-flow and proposed a model for flow rate of induced gas. In their study, the pressure on the surface of the cylindrical blade immersed in a flowing liquid was derived by application of Bernoulli's equation. More recently, Forrester and Rielly (1998) conducted an experimental study of gas bubble formation from a submerged orifice on a cylindrical, flat or concave blade section exposed to a strong liquid cross-flow. The effects of gas velocity through the orifice, liquid cross-flow velocity and blade configuration on the mode of bubble formation and bubble size at detachment were investigated.

Theoretical models for bubble formation with liquid cross-flow have been developed by Tsuge, Hibino and Nojima (1981), Kawase and Ulbrecht (1981), Morgestern and Mersmann (1982), Wace, Morrell and Woodrow (1987), Marshall, Chudacek and Bagster (1993) and Kim, Kamotani and Ostrach (1994). They are generally

* Corresponding author. Tel.: + 65-874-6360; fax: + 65-779-1936.
E-mail address: chetanbh@nus.edu.sg (R. B. H. Tan).

based either upon a force balance on the bubble or a potential flow analysis of the surrounding liquid. All these models assume spherical bubble shapes, and rely on arbitrary criteria for bubble detachment and several incorporate experimental correction factors or fitted parameters to improve the fit with their experimental data.

In Marshall et al. (1993) the spherical bubbles are assumed to grow and translate in several stages, each described by highly complex mathematical models based on spherical bubble growth using potential flow theory and the method of images. A significant drawback of this model is its inability to simulate the dynamics of neck closure; the minimum pressure criterion for detachment was used without physical justification. Furthermore, the added mass coefficient was adjusted arbitrarily to an empirical value of 0.18. The assumption of spherical bubble growth appears to be inappropriate; high-speed photographs taken during the experiments showed that the bubbles were far from spherical, with bubble elongation and deformation becoming very pronounced at higher liquid cross-flow velocities (Marshall, 1990).

Non-spherical models of bubble formation have been successful in predicting bubble formation in a quiescent liquid. In particular, the interfacial element approach employed by Marmor and Rubin (1976) and Tan and Harris (1986) has yielded good agreement with experimental results for bubble growth rate, detachment time, bubble volume at detachment and chamber pressure fluctuations. Predicted bubble shapes agree well with actual bubble shapes from experimental videotaped images. Furthermore, the interfacial element method does not rely on arbitrary detachment criteria, as detachment is simulated to occur as a result of the balance of forces acting on the bubble neck.

This paper describes a non-spherical model of bubble formation in the presence of liquid cross-flow. Model predictions are compared with the experimental results of Marshall (1990), and the analytical expressions of Wace et al. (1987) for different conditions of gas flow rate, orifice diameter and liquid cross-flow velocity.

2. Model development

The basic formulation of the model follows the interfacial element approach as described by Tan and Harris (1986) for non-spherical bubble formation in a quiescent liquid. The bubble envelope is divided into a number of small elements, with each interfacial element assigned an added mass corresponding to the cumulative volume of liquid displaced during its outward motion. An added mass coefficient having a theoretical value of 0.6875 (Milne-Thomson, 1968) was used throughout. The equations of motion for each interfacial element are solved numerically to yield the instantaneous bubble shape. Thermodynamic expressions relating the chamber and

bubble pressures and the instantaneous bubble volume are solved to provide the orifice gas flow rate. The effect of liquid motion is accounted for by the potential flow theory.

2.1. Physical system and basic equations

Fig. 1 shows the bubbling system under consideration. Gas is fed into a chamber with volume V_c , at a constant flow rate Q and pressure P_a . Gas flows through the single orifice R_o into the bubble at a flow rate q . This flow is assumed to be isothermal and incompressible and is controlled by the pressure in the chamber and that in the bubble, P_c and P_b , which are both assumed to be uniform within their volumes. A liquid flows across the bubble with a uniform velocity U_l . The following basic assumptions are made:

- The bubble remains symmetrical about its axis during the growth and is a volume of revolution around its central axis. Experimental evidence (photographic images from both side and top views) by Marshall (1990) shows that bubble shapes remain virtually symmetrical about the bubble axis even at relatively high cross-flow velocities.
- The influence of gas and liquid viscosities at the interface is negligible.
- The growth of the bubble is unaffected by the presence of other bubbles.
- The gas is ideal, isothermal and incompressible and its flow is adiabatic.
- The liquid cross-flow is isothermal, uniform, inviscid and irrotational.

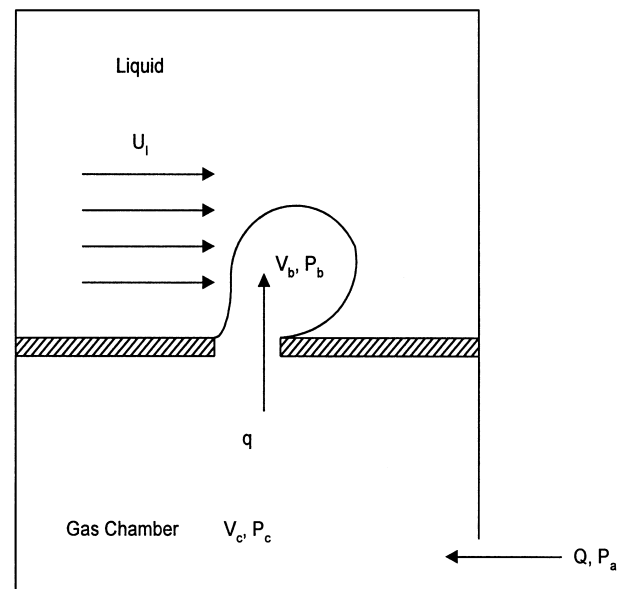


Fig. 1. Schematic diagram of the liquid cross-flow bubble formation system.

- (f) There is no energy exchange or mass transfer across the gas–liquid interface.
 (g) The non-slip boundary conditions are applied at the edge of the orifice.

Assuming an inviscid liquid, each element at the bubble interface moves as a result of forces due to pressure difference and surface tension. A force balance at each element generates a set of differential equations of motion in cylindrical coordinates:

$$r\Delta P dr - \sigma d(r \sin \beta) = \frac{d}{dt}(U_z \bar{m}), \quad (1)$$

$$r\Delta P dz + \sigma \left[d(r \cos \beta) - \frac{dz}{\sin \beta} \right] = \frac{d}{dt}(U_r \bar{m}), \quad (2)$$

where r and z are the radial coordinate from the axis of the bubble and the axial coordinate from orifice horizontal level, respectively, ΔP is the pressure difference between the bubble pressure P_b and the liquid pressure P_l at each interface element. β is an angle defined by

$$\beta = \tan^{-1} \frac{\partial z}{\partial r}. \quad (3)$$

The term \bar{m} is the added mass:

$$\bar{m} = (\alpha\rho_l + \rho_b)V_b, \quad (4)$$

where α is the added mass coefficient, taken as 0.6875, the value for a bubble moving perpendicular to the wall in an inviscid fluid (Milne-Thomson, 1968). This is regarded as an average value during the whole formation progress.

A mass balance on the chamber yields

$$V_c \frac{d\rho_c}{dt} = \rho_a Q - \rho_c q, \quad (5)$$

where ρ_c and ρ_a are the gas densities in the chamber and at supply, respectively.

From the application for the first law of thermodynamics to the chamber alone, it has been shown by Tan and Harris (1986) that

$$V_c \frac{dP_c}{dt} = \gamma(P_a Q - P_c q). \quad (6)$$

Similarly, for the system defined as the gas in the bubble and in the chamber

$$V_b \frac{dP_b}{dt} + \gamma P_b \frac{dV_b}{dt} = \gamma P_c q + (\gamma - 1) \frac{\rho_c q^3}{2a_o^2}, \quad (7)$$

where a_o is the cross-sectional area of the orifice. The last term in Eq. (7) represents a contribution from the kinetic energy of the gas through the orifice.

The orifice flow rate is given by an orifice equation of the form

$$q = C\pi R_o^2 \left[\frac{P_c - P_b}{\rho_c} \right]^{0.5}, \quad (8)$$

where C is the orifice coefficient and ρ_c is the gas density within the chamber.

The four equations (5)–(8) are easily solved for the variables P_c , P_b , ρ_c and q .

2.2. Modelling the effect of liquid cross-flow

The effect of liquid cross-flow on the bubble formation process is modelled by a combination of tilting of the bubble axis and the analysis of liquid pressure distribution on the surface of the bubble.

When a growing bubble is exposed to liquid cross-flow, expansion and horizontal translation take place. The bubble center moves normal to the liquid flow direction by the expansion process, as well as parallel to the liquid flow due to the drag force. This motion is accounted for in some existing theoretical models by the inclination of the bubble neck or axis (Sullivan et al., 1964; Kim et al., 1994) and the virtual inclination of the nozzle (Kawase & Ulbrecht, 1981). The inclination of bubble axis has been observed in the experiments of Tsuge et al. (1981) and Ghosh and Ulbrecht (1989).

In our current model, the concept of inclination of bubble axis proposed by Sullivan et al. (1964) is adopted. In the case of our non-spherical model, we assume that the bubble central axis tilts at an angle ω , which is determined by the liquid velocity, gas flow rate and bubble volume. Following the analysis of Sullivan et al. (1964), the center of the bubble moves away in the horizontal direction with a velocity U_l , the uniform velocity of the cross-flowing liquid. Therefore, the bubble is displaced by a distance of $(U_l V_b / Q)$ at any instant. Hence, the inclination of the bubble axis at any instant can be approximated by

$$\omega = \tan^{-1} \left(\frac{U_l V_b / Q}{R_{eqv}} \right), \quad (9)$$

where R_{eqv} is the equivalent radius of the non-spherical bubble.

The current situation of a uniform flow past a bubble is approximated with that of a sphere in a uniform stream. When the liquid is assumed to be inviscid and irrotational, the velocity on the interface of the spherical bubble can be easily calculated by applying the potential flow theory:

$$U = \frac{3}{2} U_l \sin \theta. \quad (10)$$

The stagnation point occurs when $\theta = 0$ or π and the velocity reaches a maximum value of $\frac{3}{2} U_l$ round the equatorial belt which is perpendicular to the direction of the stream. The liquid pressure distribution on the interface of the spherical bubble can be evaluated using Bernoulli's equation:

$$P_l + \frac{1}{2} \rho_l |U|^2 = P_\infty + \frac{1}{2} \rho_l |U_\infty|^2, \quad (11)$$

where P_∞ and U_∞ are the pressure and the velocity of the liquid at infinity, respectively. This simple concept is applied to a growing non-spherical bubble by evaluating a time-dependent θ for each interfacial element, and thereby together with tilting of the bubble axis to account for the effect of liquid cross-flow by its influence on the dynamic liquid pressure at each point on the bubble surface. This procedure will be elucidated in the following section.

2.3. Calculation of liquid pressure

The effect of liquid cross-flow on the bubble formation is modelled by the liquid pressure analysis around the bubble coupled with the concept of bubble axis inclination. As the bubble axis tilts during its formation, the flow around the bubble is altered because of the non-spherical bubble shapes. The calculation of liquid pressure distribution on the bubble surface as well as inclination of bubble axis is shown in Fig. 2.

At every time step, the angle of the bubble central axis is computed by Eq. (9). For computing efficiency, at each time step, the model simply solves for virtual bubble coordinates relative to a stationary axis of symmetry. However, in order to correctly model the effect of liquid cross-flow, the actual position of the bubble envelope with respect to the true vertical is needed. These “true” radial and axial coordinates, r_i^* and z_i^* , with respect to the true vertical are computed for each element by

$$r_i^* = \sqrt{(z_1 - z_i)^2 + r_i^2 - (z_1 \cos \omega - z_i \cos \omega - r_i \sin \omega)^2}, \quad (12)$$

$$z_i^* = z_i \cos \omega + r_i \sin \omega, \quad (13)$$

where z_1 is the z -coordinate of the top element of the bubble.

The angle θ_i for each element is then measured with respect to a horizontal line AB which is perpendicular to the true vertical and passes through the point m , which

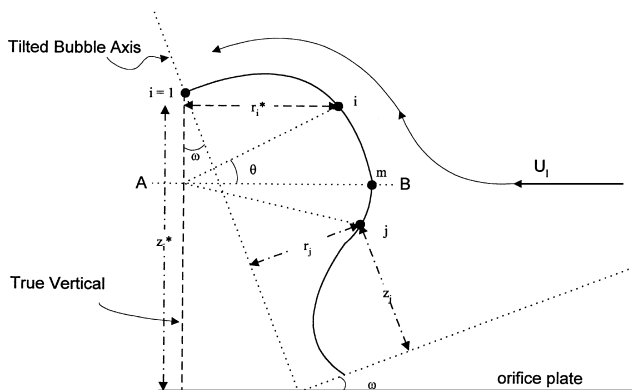


Fig. 2. Schematic diagram for calculation of liquid pressure distribution and inclination of bubble axis.

represents the outermost “point of attack” of the following liquid, or equivalently, the stagnation point. θ_i is given by

$$\theta_i = \tan^{-1} \frac{z_i^* - z_m^*}{r_i^*}, \quad (14)$$

where the subscript “m” denotes the point with a maximum r^* coordinate. Finally, the liquid pressure for each element on the bubble interface can be obtained by applying Eqs. (10) and (11).

3. Results and discussion

3.1. Comparison between bubble formation in quiescent and cross-flowing liquid

Fig. 3 shows the comparison of simulated bubble growth rate and bubble pressure fluctuation between bubble formation in quiescent and cross-flowing liquids for the air/water system, with $Q = 1.11 \text{ cm}^3/\text{s}$, $R_o = 0.125 \text{ mm}$, $V_c = 300 \text{ cm}^3$ and liquid velocities at 0.0, 0.6, and 1.2 m/s. From Fig. 3(a), it can be observed that bubble growth begins immediately in a flowing liquid, whereas there is a short delay for the case of a quiescent liquid. This is due to lower liquid pressures in the case of a flowing liquid (Eq. (11)) and therefore a comparatively greater initial driving force for bubble growth. However, once a bubble begins rapid growth, it appears that the initial growth rates are similar for both quiescent

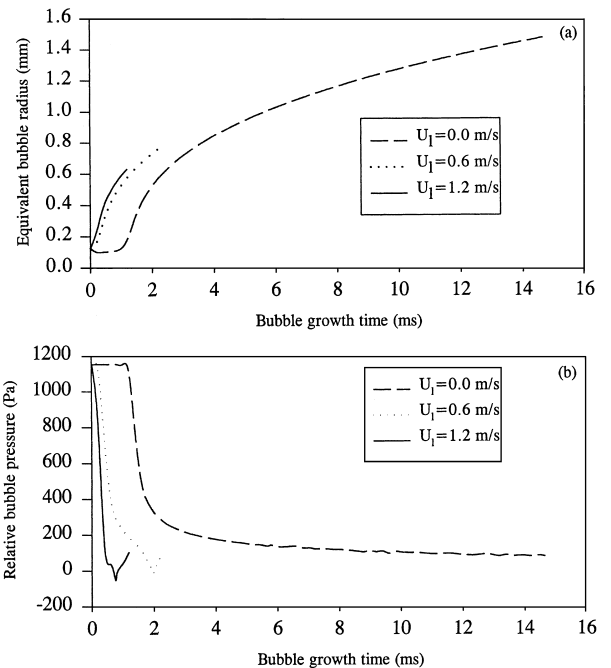


Fig. 3. Simulated bubble growth: comparison of bubble growth rate and bubble pressure fluctuation between bubble formation in quiescent and cross-flowing liquids.

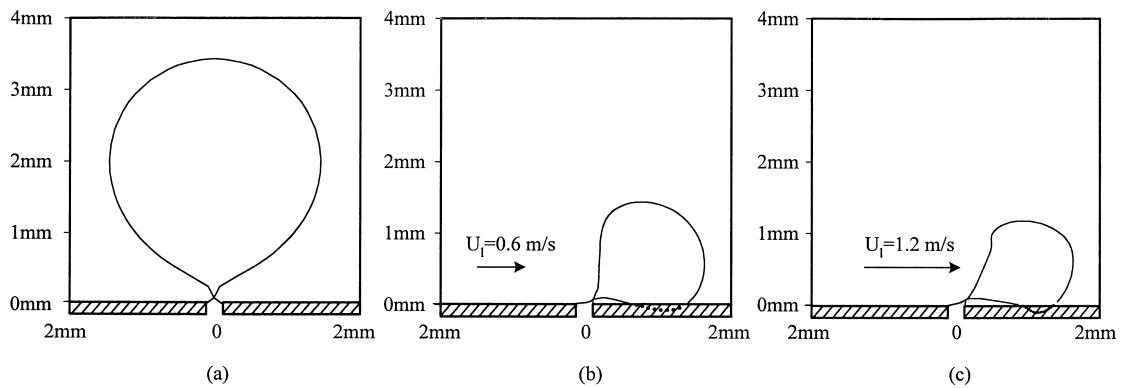


Fig. 4. Simulated final bubble shapes for quiescent liquid and cross-flowing liquid bubble formation. System = air/water, $Q = 1.11 \text{ cm}^3/\text{s}$, $R_o = 0.125 \text{ mm}$, $V_c = 300 \text{ cm}^3$ and $U_l = 0.0, 0.6$ and 1.2 m/s .

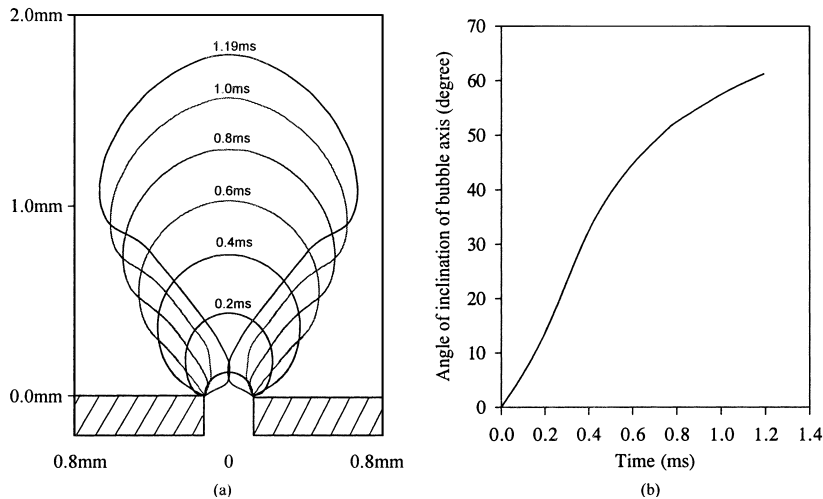


Fig. 5. (a) Computed bubble shapes without the tilting of bubble vertical axis, (b) Variation of angle of inclination of bubble vertical axis with time during bubble formation.

and cross-flowing liquids, as can be seen from Fig. 3(a). It is obvious that termination of the bubble formation process (i.e. detachment) occurs much sooner in the simulations with liquid cross-flow. The reason for this can be deduced from Fig. 3(b), which compares the relative bubble pressures (i.e. the difference between the bubble pressure and the stagnation pressure at orifice) during bubble formation. In the case of bubble formation in the presence of liquid cross-flow, the very low bubble pressures caused by rapid bubble growth occur much sooner. In the interfacial element model formulation, low bubble pressure is the dynamic driving force for neck formation and closure. The earlier detachment of bubbles due to a cross-flowing liquid has been clearly demonstrated in the experiments of Morgenstern and Mersmann (1982).

The corresponding final bubble shapes are shown in Fig. 4. Apart from the influence of liquid velocity on bubble size, it can be observed that the cross-flow velocity has an appreciable effect on the simulated bubble shapes. While the simulated bubble formed in quiescent

liquid is nearly spherical, the one in a cross-flowing liquid had been displaced downstream and deviates from a spherical shape.

3.2. Evolution of bubble shape during formation

The procedure by which the simulated bubble shapes and orientation are computed is illustrated in Fig. 5 for the case of air/water, $Q = 1.11 \text{ cm}^3/\text{s}$, $R_o = 0.125 \text{ mm}$, $V_c = 300 \text{ cm}^3$ and $U_l = 1.2 \text{ m/s}$ which are the experimental conditions of run EHS011 in Marshall's (1990) thesis. Fig. 5(a) shows the computed bubble shapes as solved by our model along the untilted axis. Physically, the bubble would have tilted by an angle ω . Fig. 5(b) shows that the variation of angle of inclination increases from 0 to 61.2° during the formation process. The model solves the force balance equations based on the actual tilted coordinates. The corresponding actual bubble shapes and orientations during the simulated bubble growth sequence are shown in Fig. 6, which are in very

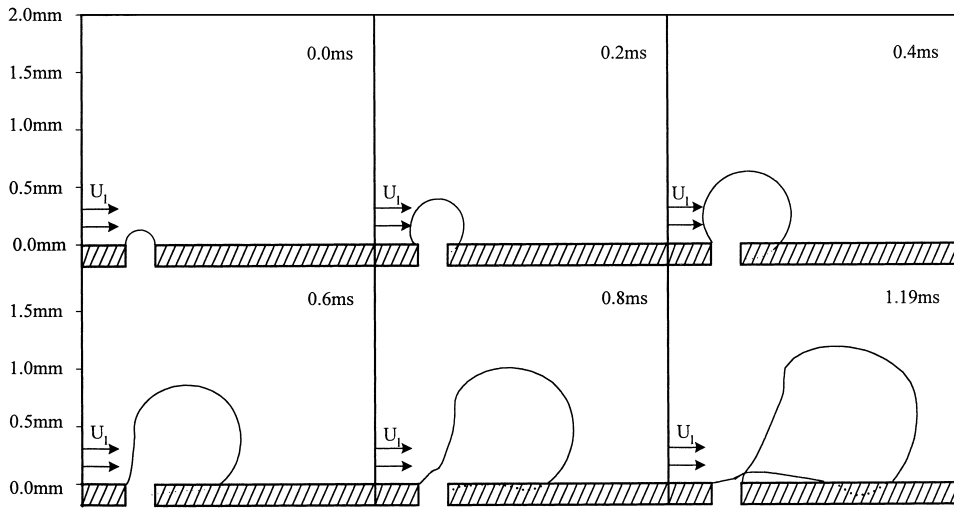


Fig. 6. Computed bubble growth sequence for experimental conditions of run EHS011 from Marshall (1990). System = air/water, $Q = 1.11 \text{ cm}^3/\text{s}$, $R_o = 0.125 \text{ mm}$, $V_c = 300 \text{ cm}^3$ and $U_i = 1.2 \text{ m/s}$.

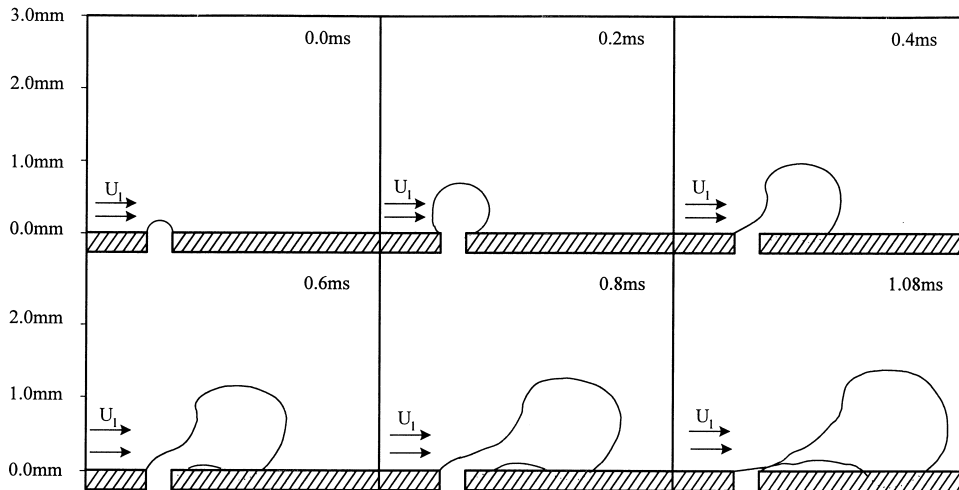


Fig. 7. Computed bubble growth sequence for the experimental conditions of run EHS021B from Marshall (1990). System = air/water, $Q = 2.22 \text{ cm}^3/\text{s}$, $R_o = 0.175 \text{ mm}$, $V_c = 300 \text{ cm}^3$ and $U_i = 2.4 \text{ m/s}$.

good agreement with the experimental video images taken by Marshall (1990).

Fig. 7 shows an example of bubble formation with high liquid cross-flow velocity; the conditions are: air/water, $Q = 2.22 \text{ cm}^3/\text{s}$, $R_o = 0.175 \text{ mm}$, $V_c = 300 \text{ cm}^3$ and $U_i = 2.4 \text{ m/s}$, corresponding to experimental run EHS021B in Marshall (1990). The evolution of an elongated bubble neck is predicted, as is clearly evidenced in the experimental high-speed movie sequences reported by Marshall (1990).

Due to the tilting of the bubble vertical axis, parts of the simulated bubble envelope may become displaced below the orifice, as shown in Figs. 6 and 7. This phenomenon is clearly impossible in reality. When this occurs in our model, the growing bubble can be regarded as lying against the orifice plate. When the displacement of

bubble below the orifice plate occurs in modelling, the actual bubble shape becomes somewhat uncertain, especially towards the end of its growth for large tilt angles.

The corresponding experimental sequences reported by Marshall (1990) show the bubble shape spreading over the orifice plate as it grows. While this occurrence clearly affects the assumption of symmetry about the bubble axis, resulting in some uncertainty with regard to the simulated bubble shapes, the effect on predicted bubble volume is relatively small (a maximum of 1 and 3% for the cases in Figs. 6 and 7, respectively).

A further minor difficulty arises when the bubble axis is very inclined in that the base of the predicted bubble is not attached to the orifice. A small correction is required to draw the correct bubble shape, but the effect on bubble volume is negligible. On the other hand, the realistic

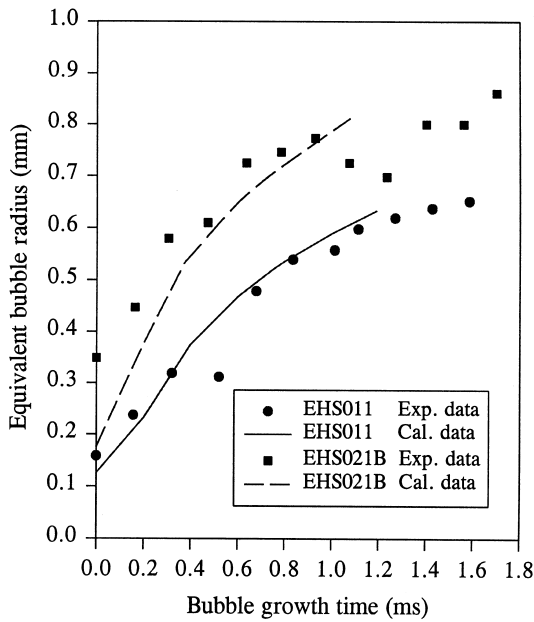


Fig. 8. Bubble growth rates for the experimental conditions of runs EHS011 and EHS021B from Marshall (1990).

bubble orientations predicted by our model (as shown in Figs. 6 and 7) demonstrate the appropriateness of the “tilting axis” approach in modelling the effect of liquid cross-flow on bubble formation.

3.3. Bubble growth rates

Simulated and the experimental bubble growth rates for bubble formation at conditions corresponding to those in Figs. 6 and 7 (Marshall, 1990, runs EHS011 and EHS021B, respectively) are plotted in Fig. 8. In the former case, the instantaneous bubble volumes predicted from our model agree very well with the experimental data. The predicted detachment occurs somewhat earlier than that in the experiment, but the final bubble volume at detachment is virtually the same. In the latter case (EHS021B), the discrepancy in detachment time is more marked. Marshall (1990) reported difficulties in determining experimentally the precise point of detachment, especially at high liquid cross-flow velocities, due to uncertainty in interpreting the video images. Furthermore, run EHS021B may be an instance of delayed release, in which the bubble remains attached to the orifice for an extended period prior to detachment (McCann & Prince, 1971). In view of the above uncertainties, the model predicts the bubble growth curves reasonably well.

3.4. Variation of bubble volume with cross-flow velocity

Fig. 9 shows the variation of bubble departure radius with liquid cross-flow velocity for the conditions

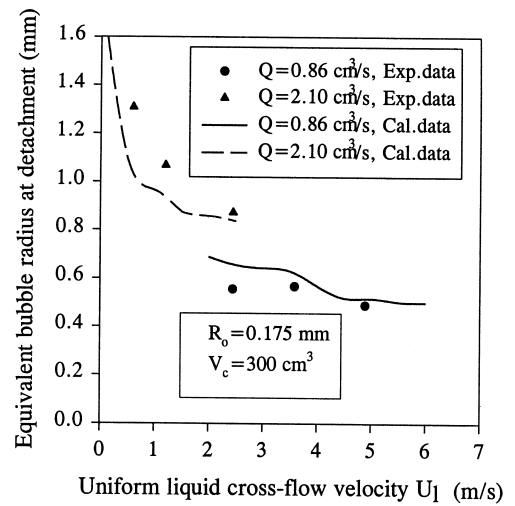


Fig. 9. Variation of bubble equivalent radius at detachment with liquid cross-flow velocity. Experimental data from Marshall (1990).

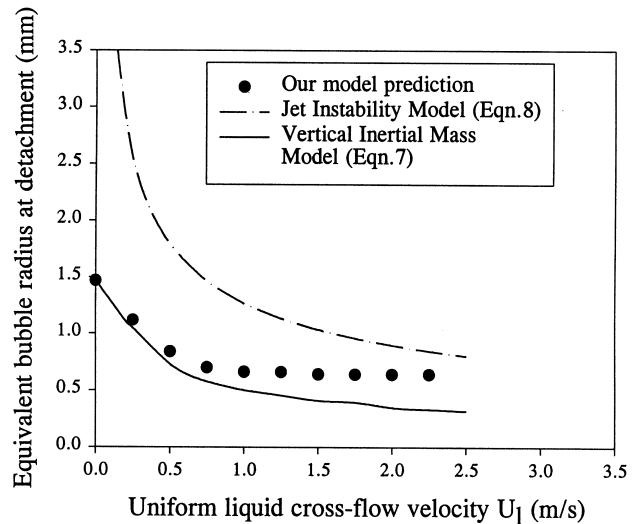


Fig. 10. Comparison with the model predictions with analytical expressions for maximum and minimum bubble sizes derived by Wace et al. (1987).

air/water, $R_o = 0.175$ mm, $V_c = 300$ cm³ and $Q = 0.86$ and 2.10 cm³/s. Simulated results are compared with the limited experimental data available (Marshall, 1990) for the influence of cross-flow velocity on bubble volumes at the two values of gas flowrate. It can be seen that the model predictions follow the experimental trends rather well within the regions studied.

Wace et al. (1987) derived a theoretical expression for the minimum bubble size for bubble formation in liquid cross-flow by considering only the vertically acting hydrodynamic mass:

$$V_b^{8/3} + V_b^{4/3} \left(\frac{U_1}{Q} \right)^2 \left(\frac{4\pi}{3} \right)^{2/3} V_q^{8/3} = V_q^{8/3}, \quad (15)$$

where V_q is the final bubble volume formed in quiescent liquid under the same experimental conditions.

In the same work, the authors also considered the jet instability model of Rayleigh (1879) in the simple form

$$R_{eqv,max} = 1.2 \sqrt{\frac{Q}{U_l}} \quad (16)$$

and regard it as predicting a maximum value for the bubble size.

Fig. 10 shows a plot of equivalent bubble radius predicted by Eqs. (15) and (16) together with results from our model for a typical set of conditions ($Q = 1.11 \text{ cm}^3/\text{s}$, $R_o = 0.125 \text{ mm}$, $V_c = 300 \text{ cm}^3$). It is clear that our model predictions fall within the upper and lower bounds considered by Wace et al. (1987). Our simulated results are seen to follow Eq. (15) for low liquid velocities, where vertical inertial terms are dominant, and to converge towards Eq. (16) for liquid cross-flow velocities, at which jet instability can be considered as the significant mechanism of bubble detachment.

4. Conclusion

A new model for non-spherical bubble formation with liquid cross-flow has been developed. The model predicts physically realistic bubble shapes, bubble growth rates and detachment times. Simulated results agree well with the limited experimental data available in the literature.

Notation

a_o	cross-sectional area of the orifice, m^2
C	orifice coefficient, dimensionless
\bar{m}	added mass, kg
P_a	gas pressure at inlet to chamber, Pa
P_b	gas pressure within bubble, Pa
P_c	gas pressure within chamber, Pa
P_l	liquid pressure at interfacial element, Pa
P_∞	liquid pressure at infinity, Pa
q	gas flow rate through orifice, m^3/s
Q	gas flow rate into chamber, m^3/s
r	radial coordinate from axis of bubble, m
r^*	true radial coordinate with respect to the true vertical, m
R_o	orifice radius, m
R_{eqv}	equivalent radius of non-spherical bubble at any instant, m
$R_{eqv,max}$	maximum equivalent bubble departure size, m
U	velocity of interfacial element, m/s
U_l	uniform liquid cross-flow velocity, m/s

U_∞	liquid velocity at infinity, m/s
V_b	bubble volume at any instant, m^3
V_c	chamber volume, m^3
V_q	final bubble volume formed in quiescent liquid, m^3
z	axial coordinate from bubble base, m
z^*	true axial coordinate with respect to orifice plate, m
z_1	z-coordinate of the top of bubble

Greek letters

α	added mass coefficient, dimensionless
β	angle defined in Eq. (3)
γ	adiabatic gas constant, dimensionless
θ	angle defined in Fig. 2, dimensionless
ω	angle of inclination of bubble vertical axis due to liquid cross-flow, dimensionless
ρ_a	gas density at supply, kg/m^3
ρ_b	gas density within bubble, kg/m^3
ρ_c	gas density within chamber, kg/m^3
ρ_l	liquid density, kg/m^3
Φ	velocity potential function

References

- Forrester, S. E., & Rielly, C. D. (1998). Bubble formation from cylindrical, flat and concave sections exposed to a strong liquid cross-flow. *Chemical Engineering Science*, 53(8), 1517–1527.
- Ghosh, A. K., & Ulbrecht, J. J. (1989). Bubble formation from a sparger in polymer solutions-II. Moving liquid.. *Chemical Engineering Science*, 44, 969–977.
- Kawase, Y., & Ulbrecht, J. J. (1981). Formation of drops and bubbles in flowing liquids. *Industrial and Engineering Chemistry, Process Design and Development*, 20(4), 636–640.
- Kim, I., Kamotani, Y., & Ostrach, S. (1994). Modeling bubble and drop formation in flowing liquids in microgravity. *AIChE Journal*, 40(1), 19–28.
- Maier, C. G. (1927). Producing small bubbles of gas in liquids by submerged orifices. *US Bureau of Mines Bulletin*, 260, 62–121.
- Marmur, A., & Rubin, E. (1976). A theoretical model for bubble formation at an orifice submerged in an inviscid liquid. *Chemical Engineering Science*, 31, 453–463.
- Marshall, S. H. (1990). *Air bubble formation from an orifice with liquid cross-flow*. Ph.D. thesis, University of Sydney, Australia.
- Marshall, S. H., Chudacek, M. W., & Bagster, D. F. (1993). A model for bubble formation from an orifice with liquid cross-flow. *Chemical Engineering Science*, 48, 2049–2059.
- McCann, D. J., & Prince, R. G. H. (1971). Regimes of bubbling at a submerged orifice. *Chemical Engineering Science*, 26, 1505–1512.
- Milne-Thomson, L. M. (1968). *Theoretical hydrodynamics* (5th ed.) (pp. 487–489) London: Macmillan.
- Morgenstern, I. B., & Mersmann, A. (1982). Aeration of highly viscous liquids. *German Chemical Engineering*, 5, 374–379.
- Rayleigh, J. W. S. (1879). On the stability of jets. *Proceedings of the London Mathematical Society*, 10, 4–29.

- Rigby, C. D., Evans, G. M., & Jameson, G. J. (1995). Modelling of gas flow from a submerged orifice in liquid cross-flow. *Transactions of the Institution of Chemical Engineers*, 73(A), 234–240.
- Stich, K., & Barr, A. (1979). Begasung Querströmenden Wassers durch einzelund mehrfachöffnungen sehr kleiner Durchmesser [gas injection into crossflowing water through single and multiple orifices of very small diameter]. *Vehrfahrenstechnik*, 9, 671–681.
- Sullivan, S. L., Hardy, B. W., & Holland, C. D. (1964). Formation of air bubbles at orifices submerged beneath liquids. *A.I.Ch.E. Journal*, 10(6), 848–854.
- Tan, R. B. H., & Harris, I. J. (1986). A model for non spherical bubble growth at a single orifice. *Chemical Engineering Science*, 41(12), 3175–3182.
- Tsuge, H., Hibino, S., & Nojima, U. (1981). Volume of a bubble formed at a single submerged orifice in a flowing liquid. *International Chemical Engineering*, 21(4), 630–636.
- Wace, P. F., Morrell, M. S., & Woodrow, J. (1987). Bubble formation in a transverse horizontal liquid flow. *Chemical Engineering Communications*, 62, 93–106.